Facile Fabrication of Hollow Tubular Mixed Oxides for Selective Catalytic Reduction of NO_x at Low Temperature: A Combined Experimental and Theoretical Study

Xiuyun Wang[a], Zhixin Lan[a], Yi Liu[a], Yongjin Luo[b*], Jianjun Chen[a], Lilong Jiang[a*] and Yong Wang[c*]

[a]*National Engineering Research Center of Chemical Fertilizer Catalyst, Fuzhou University,Fuzhou, Fujian 350002, China.*

[b]*College of Environmental Science and Engineering, Fujian Normal University, Fuzhou 350007, China.*

[c]*Voiland School of Chemical Engineering and Bioengineering, Washington State University, Pullman, WA 99164, USA.*

Experimental Section

The preparation of $CuMn_2O_4$, $CoMn_2O_4$, $NiMn_2O_4$, $NiCo_2O_4$, $FeCo_2O_4$ and $CuCo_2O_4$ nanostructures involves two steps. Taking $CuCo_2O_4$ as an example, 0.4 mmol $Cu(NO_3)_2{\cdot}3H_2O$, 0.8 mmol $Co(NO_3)_2{\cdot}6H_2O$, 1.44 mmol citric acid (CA) and 1.2 g polyacrylonitrile were dissolved in 19 mL of dimethylformamide solvent. The applied voltage, feeding rate, and distance between the stainless steel needle and collector were 18 kV, 1.0 mL/h and 22 cm, respectively. Then, the obtained PAN@$CuCo_2O_4$ precursor was calcined at 400 ^oC for 2 h. By simply changing the heating rate from 0.5 to 10 ^oC/min, the nanostructures of $CuCo_2O_4$ can be tuned from hollow tube to 1D solid structure. The obtained catalysts were labeled as $CuCo_2O_4$-0.5 (0.5 ^oC/min), $CuCo_2O_4$ (1 ^oC/min), $CuCo_2O_4$-3 (3 ^oC/min), $CuCo_2O_4$-5 (5 ^oC/min) and $CuCo_2O_4$-solid (10 ^oC/min), respectively. The synthesis process of other mixed metal oxides with hollow tubular structure or 1D solid nanowire, such as $NiCo_2O_4$, $FeCo_2O_4$, $CuMn_2O_4$, $CoMn_2O_4$ and $NiMn_2O_4$ is similar to that of $CuCo_2O_4$ except for using different raw materials of nitrate.

Catalytic activity tests

SCR activity measurement was performed in a fixed-bed stainless steel reactor (inner diameter = 8 mm). Before each test, 0.2 g of sample was pretreated by 5 vol% H_2/Ar at 400 ^oC for 2 h. After cooled to test temperature, the feed gas (335 ppm NO, 340 ppm NH_3 and 2 vol% O_2 balanced with Ar) was introduced using mass-flow

controllers, and the total flow rate was kept at 600 mL/min. and the gas hourly space velocity (GHSV) is 150, 000 h^{-1}. Besides, hollow tubular $CuCo_2O_4$ was also tested in a wide GHSV including 200,000, 250,000, 300,000 and 400,000h^{-1}). Resistance against H_2O was examined through introducing 7 vol% H_2O into feed gas at 250 ^oC. SO_2 poisoning experiment was carried out by exposing samples to feed gas containing additional 100 ppm SO_2 at 250 °C. Stability tests of hollow tubular $CuCo_2O_4$ and $CuCo_2O_4$-solid were performed at 400 ^oC for 30 h. The outlet NO_x concentration was monitored by an on-line chemiluminescence NO-NO_2-NO_x analyzer (Model 42i-HL, Thermo Scientific). The outlet N_2O was analyzed using an FTIR spectrometer (Nicolet Nexus 6700) with a heated, multiple-path gas cell. NO_x conversion under steady-state conditions for 1 h was calculated according to the following equation.

NO_x conversion (%) = ($NO_{x\ inlet}$ - $NO_{x\ outlet}$)/ $NO_{x\ inlet}$ ×100%

Transient response method (TRM) of hollow tubular $CuCo_2O_4$ was carried out at 150 ^oC according to literature methods [1, 2]. A 0.1 g sample was firstly pretreated in air flow (30 mL/min) at 400 ^oC for 0.5 h. After cooling to 150 ^oC, 250 ppm NO was introduced and the reactor was maintained at steady state for 30 min, then a feed gas of 250 ppm NO, 1 vol% O_2 and 250 ppm NH_3 balanced by Ar were introduced in the next step. The outlet gas concentrations were continuously monitored by a mass spectrometer and UV analyzer.

Catalyst characterization

X-ray diffraction (XRD) patterns were recorded on a RIGAKU-Miniflex II X-ray diffractometer with Cu K_α radiation (λ = 1.5406 Å). N_2 physisorption measurement was performed on an ASAP 2020 apparatus, the sample was degassed in vacuo at 180 ^oC at least 6 h before the measurement. Field Emission Scanning Electron Microscope (FESEM) was performed on JSM6700-F. Transmission Electron Microscope (TEM) and high-resolution transmission electron microscopy (HRTEM) measurements were carried out on a JEM-2010 microscope operating at 200 kV in the mode of bright field. X-ray photoelectron spectroscopy (XPS) analysis was performed on Physical Electronics Quantum 2000, equipped with a monochromatic Al-K_α source (K_α = 1,486.6 eV) as a radiation source at 300 W under UHV. Catalyst charging during the measurement was compensated by an electron flood gun. High-resolution spectra were acquired with a pass energy of 20 eV. The area of analysis was 700 × 300 μm in size, and each sample was analyzed at a 90° takeoff angle with a depth of 3-4 nm.

H_2 temperature-programmed reduction (H_2-TPR) was performed on AutoChem II 2920 equipped with a TCD detector, in which the sample was pretreated under air flow (30 mL/min) at 400 ^oC for 0.5 h, followed by purging with Ar (30 mL/min) at the same temperature for 0.5 h, and then cooled down to 50 ^oC. H_2-TPR was started from 50 to 800 ^oC under 10 vol% H_2/Ar.

Oxygen temperature-programmed desorption (O_2-TPD) was conducted on an AutoChem 2920 equipped with a TCD detector. The adsorption of O_2 was performed in a 4% O_2 /He gas flow for 1 h at 150 ^oC. Afterward, the sample was heated to 900 °C at a heating rate of 1 °C/min in a pure He gas flow. O_2-TPD quadruple mass spectroscopy (Q-MS) was used to analyze evolving gases. The signals for O_2 (m/z = 32), H_2O (m/z= 18), and CO_2 (m/z=44) were monitored by using a QIC20 bench top gas analysis system connected to an AutoChemII 2920 outlet.

Ammonia temperature-programmed desorption (NH_3-TPD) was also conducted on the AutoChem 2920 equipped with a TCD detector. 0.1 g of sample was pretreated in Ar at 350 ^oC for 1h. After cooled to 50 ^oC, the sample was exposed to 1.0 vol% NH_3/Ar for 0.5 h, followed by a Ar purge at 100 ^oC to remove physisorbed ammonia. Finally, NH_3-TPD was measured from 50 to 1000 ^oC.

In situ diffuse reflection infrared Fourier transform spectroscopy (DRIFTS) was recorded on a Nicolet Nexus FT-IR spectrometer in the range of 650-4000 cm^{-1} with 32 scans at a resolution of 4 cm^{-1}. Prior to each experiment, the sample was pretreated at 350 ^oC for 0.5 h in a gas flow of N_2 to remove any adsorbed impurities, and then cooled down to 50 ^oC. The background spectrum was collected under N_2 and automatically subtracted from the sample spectra. Afterward, NH_3 (500 ppm balanced with Ar) was introduced to the cell in a flow rate of 30 mL/min at 100^oC for 1 h to ensure complete absorption saturation. After physisorbed ammonia was removed by flushing wafer with N_2 at 100 ^oC for 3 h, DRIFTS spectra were recorded at 50-350 ^oC. After NH_3 adsorption, the catalyst was pretreated at 200 °C under an N_2 flow with 20 mL/min for 1 h, subsequently 500 ppm of NO + 5 vol % O_2/Ar (20 mL/min) were introduced to investigate the reactivity of pre-adsorbed NH_3 with NO + O_2 species.

All spin-polarized DFT calculations were carried out using the Vienna ab Initio Simulation Program (VASP) with the gradient-corrected PW91 exchange-correction function. For valence electrons, a tight convergence of the plane-wave expansion was obtained with a kinetic energy cutoff of 500 eV, and the ionic cores were described

with the projector augmented-wave (PAW) method. The Brillouin zone of the Monkhorst−Pack grid was set at 2 × 2 × 1. For energy calculation, the electronic energy was converged to 10^{-5} eV, and the positions of the atoms were allowed to relax until all forces were smaller than 0.02 eV/ Å. The O_2 adsorption ability is defined by using adsorption energy term (E_{ads}), which is calculated according to $E_{ads} = E_{(surface+gas)} - E_{surface} - E_{gas}$. $E_{(surface+gas)}$, $E_{surface}$ and E_{gas} are the total energy of the optimized adsorbate surface system, energy of the naked surface and energy of a gas molecule, respectively. The energy of oxygen vacancy formation (E_v) was calculated according to $E_v = E_{oxygen\ vacancy\ system} + 1/2E_{O2} - E_{full\ system}$, this formula assumes that the oxygen atoms leaving the surface combine to form the oxygen molecule. $E_{oxygen\ vacancy\ system}$, E_{O2}, and $E_{full\ system}$ are the energy of the oxygen vacancy system, energy of an oxygen molecule, and energy of the full system, respectively.

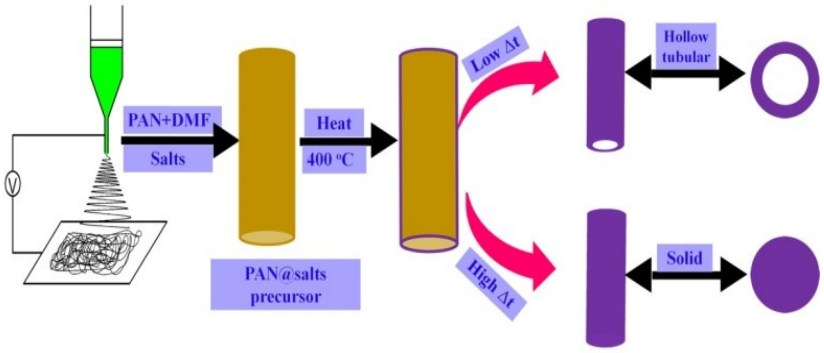

Figure S1 Synthetic route of $CuCo_2O_4$ with hollow tubular and solid 1D nanostructure.

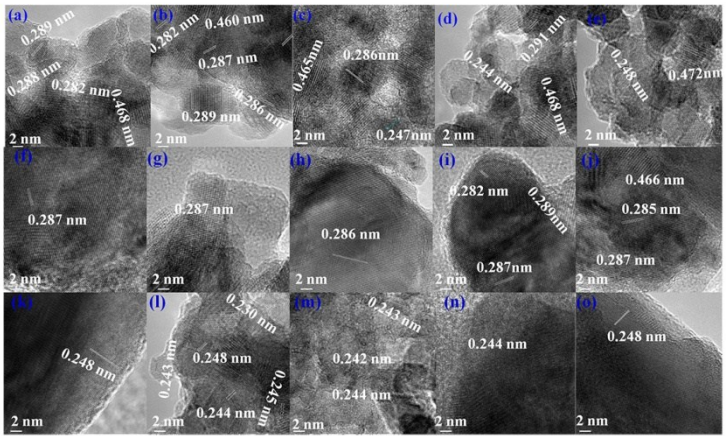

Figure S2 HRTEM images of (a) $CuCo_2O_4$-0.5; (b, f, g, h, i, j) $CuCo_2O_4$ ($CuCo_2O_4$-1); (c) $CuCo_2O_4$-3; (d) $CuCo_2O_4$-5 and (e, k, l, m, n, o) $CuCo_2O_4$-solid ($CuCo_2O_4$-10).

HRTEM images {Figure S2 (b, f, g, h, i, j)} show that the spacing distances between two fringes in hollow tubular $CuCo_2O_4$ ($CuCo_2O_4$-1) are 0.282-0.289 and 0.460 nm, matching with (220) and (111) planes, respectively. For $CuCo_2O_4$-solid {Figure S2 (e, k, l, m, n, o)}, the lattice spacing of 0.242-0.248 and 0.472 nm correspond to (311) and (111) crystal planes, respectively, while the lattice spacing of 0.230 nm corresponds to (222) plane.

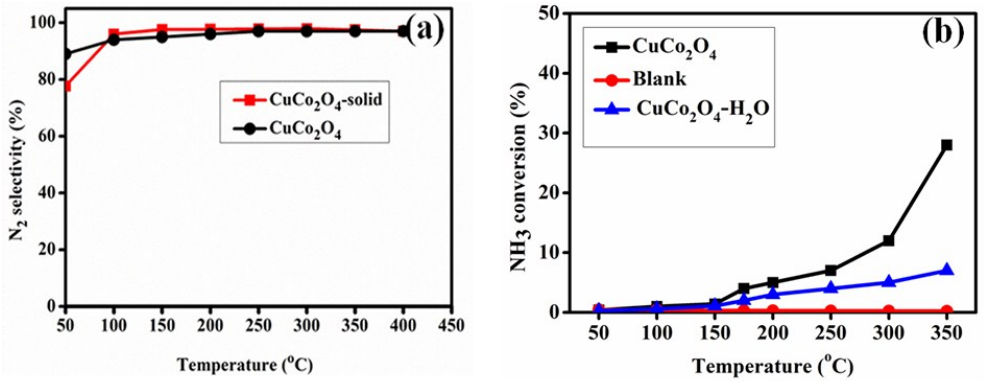

Figure S3 a) N_2 selectivity of hollow tubular $CuCo_2O_4$ and $CuCo_2O_4$-solid at different temperatures; b) NH_3 conversion in separates NH_3 oxidation reaction of $CuCo_2O_4$. Reaction condition: 40 ppm of NH_3, 2 vol % O_2, Ar as balance gas.

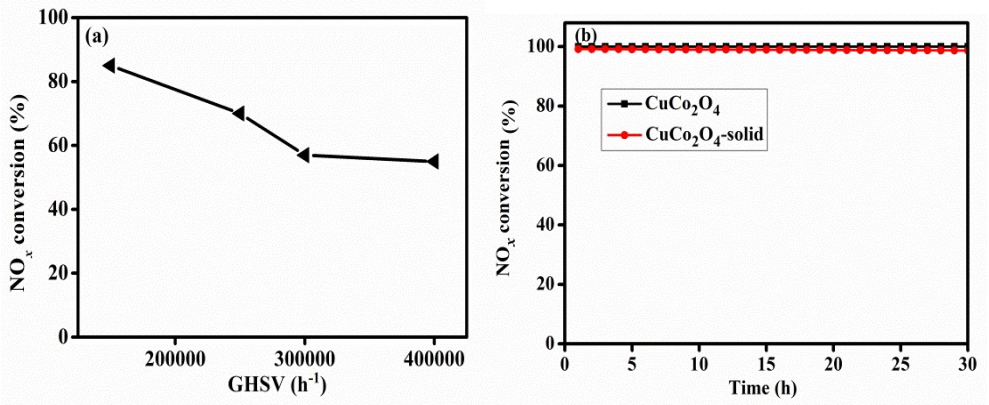

Figure S4 a) Influence of GHSV on NO_x conversion in hollow tubular $CuCo_2O_4$ at 150 ^{o}C; b) Stability of $CuCo_2O_4$ and $CuCo_2O_4$-solid at 400 ^{o}C;

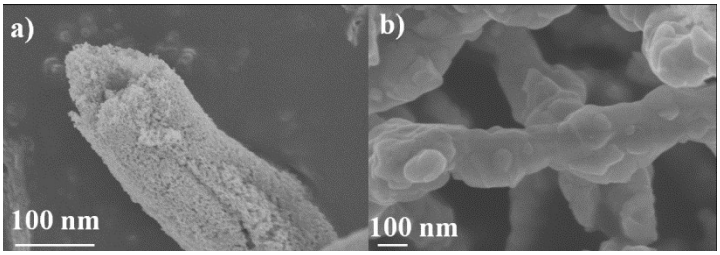

Figure S5 SEM images of (a) hollow tubular $CuCo_2O_4$ and (b) $CuCo_2O_4$-solid after NH_3-SCR activity test.

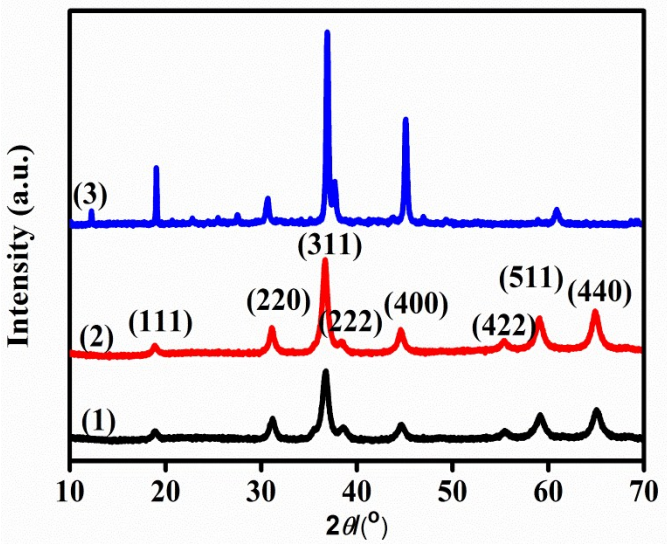

Figure S6 XRD patterns of (1) $CuCo_2O_4$-solid, (2) hollow tubular $CuCo_2O_4$ and (3) hollow tubular $CuCo_2O_4$ after activity test.

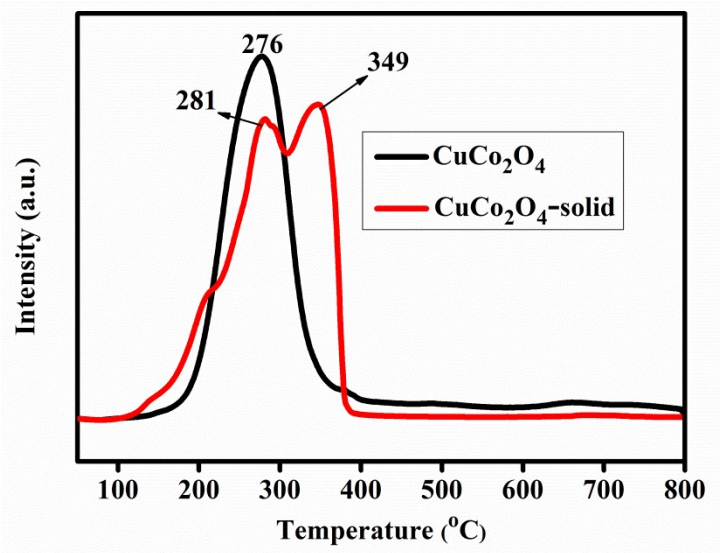

Figure S7 H_2-TPR profiles of hollow tubular $CuCo_2O_4$ and $CuCo_2O_4$-solid.

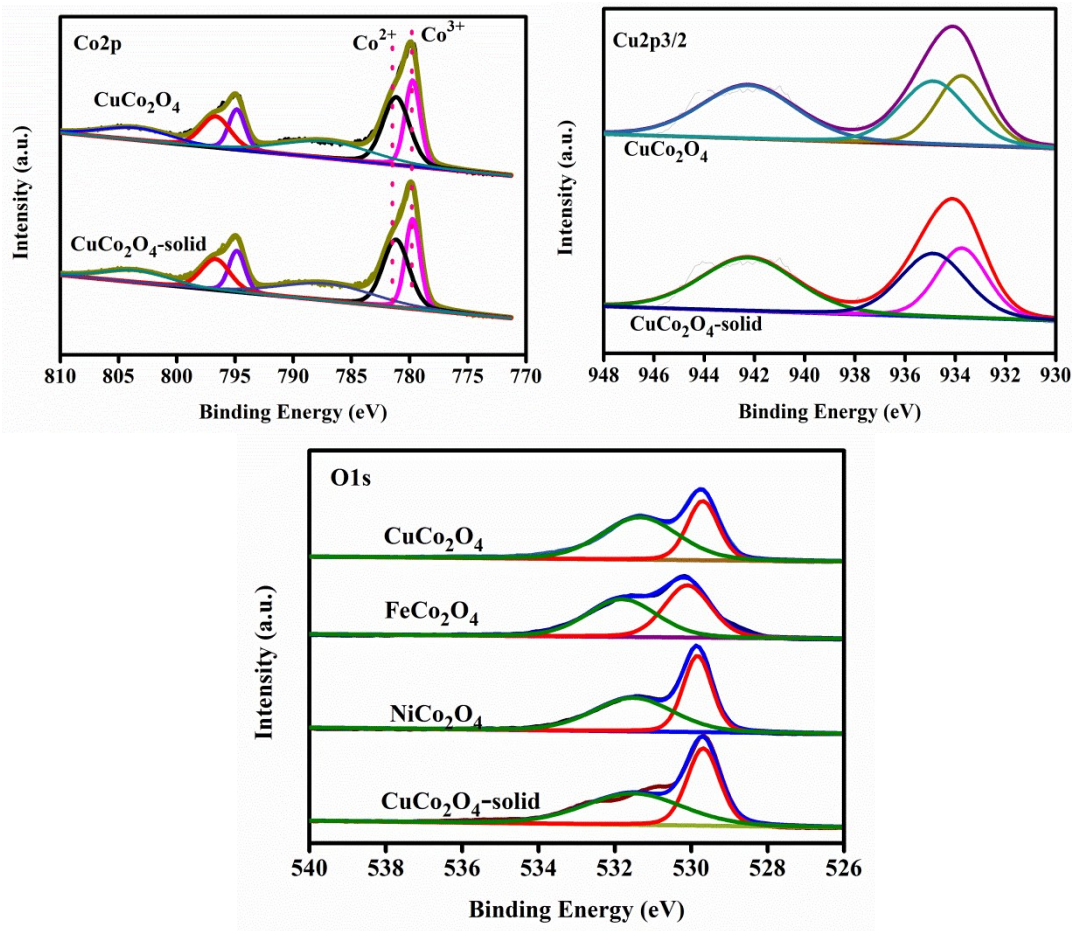

Figure S8 XPS spectra of Cu 2p, Co 2p and O 1s.

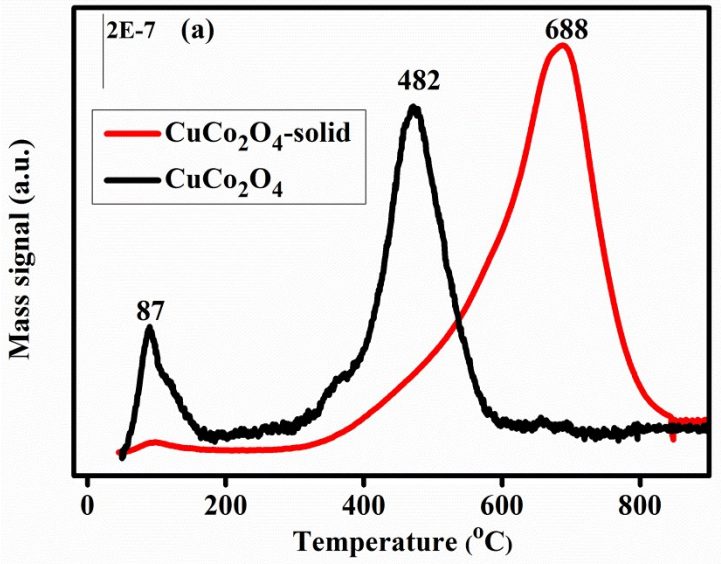

Figure S9 O_2-TPD-MS profiles of hollow tubular $CuCo_2O_4$ and $CuCo_2O_4$-solid.

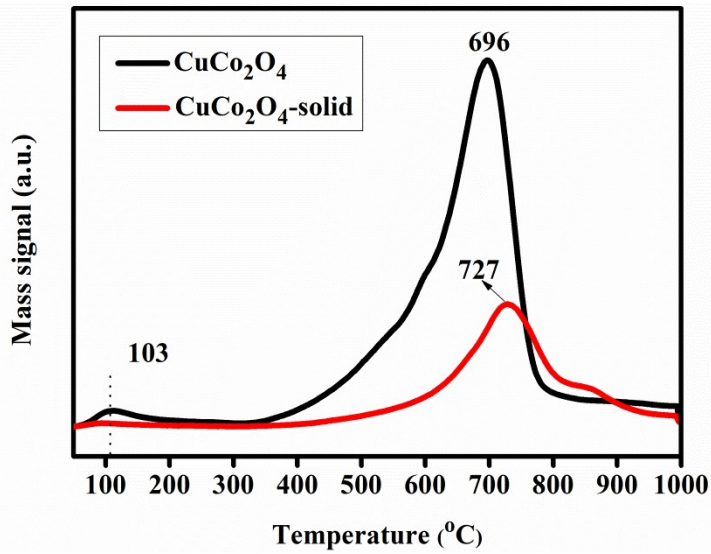

Figure S10 NH_3-TPD-MS profiles of hollow tubular $CuCo_2O_4$ and $CuCo_2O_4$-solid.

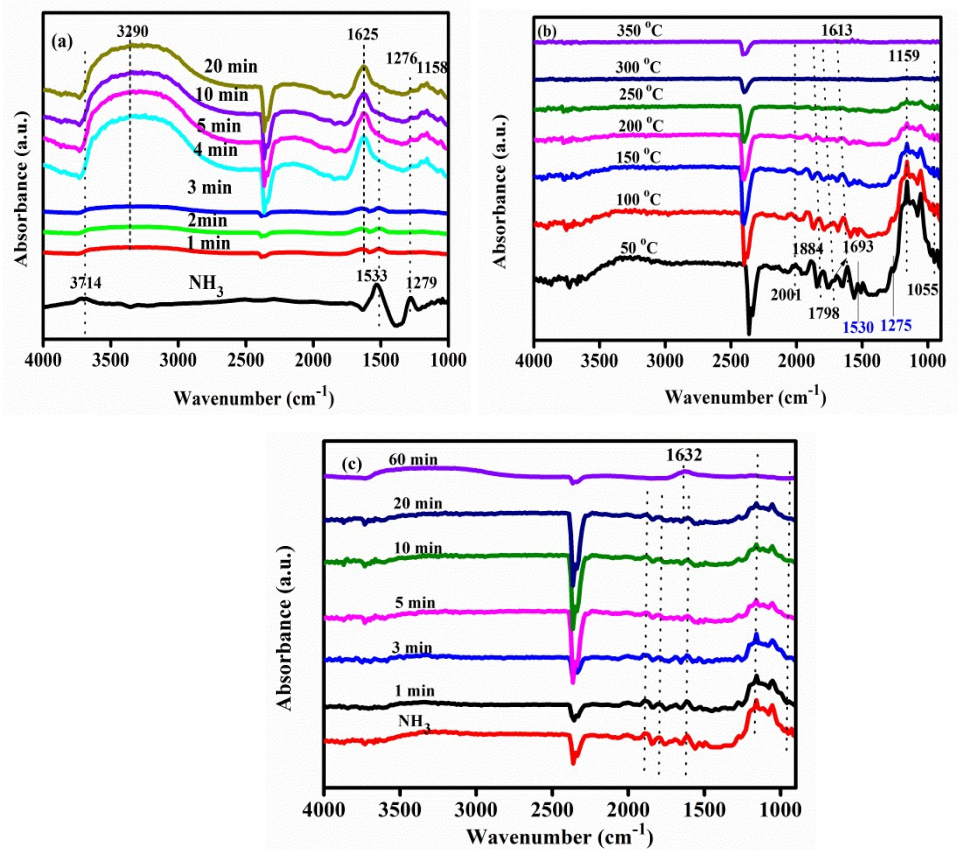

Figure S11 *In situ* DRIFT spectra of NO + O_2 react with pre-adsorbed NH_3 species at 200 °C on $CuCo_2O_4$ hollow tubular (a) and $CuCo_2O_4$-solid (c); (b) NH_3 adsorption at different temperatures over $CuCo_2O_4$-solid.

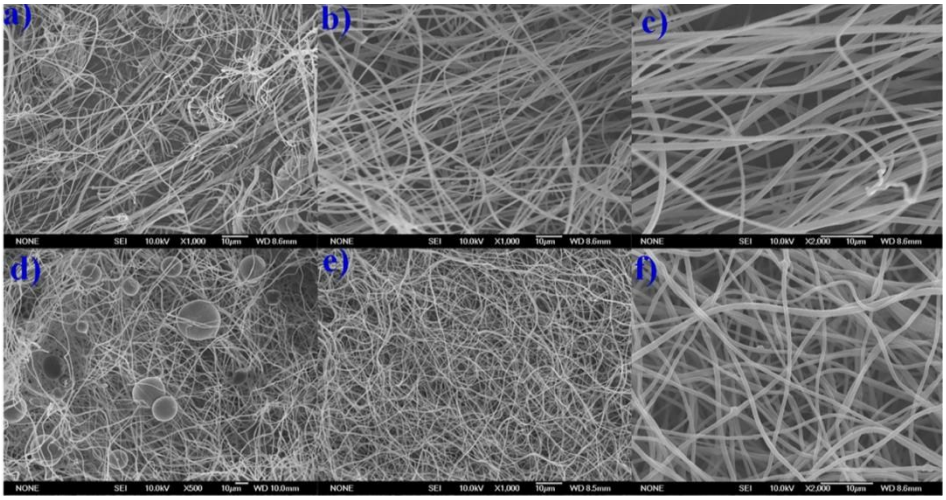

Figure S12 SEM images of a) PAN@$NiMn_2O_4$; b) PAN@$CuMn_2O_4$; c) PAN@$CoMn_2O_4$; d) PAN@$FeCo_2O_4$; e) PAN@$NiCo_2O_4$ and f) PAN@$CuCo_2O_4$.

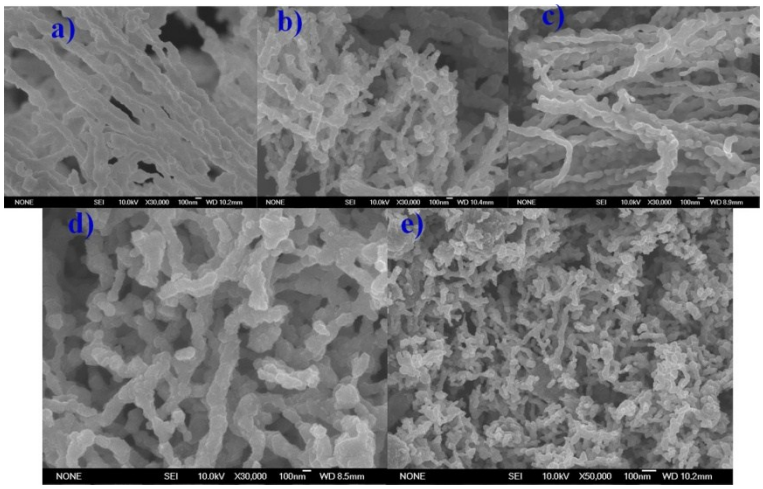

Figure S13 SEM images of a) $NiMn_2O_4$-solid; b) $CuMn_2O_4$-solid; c) $CoMn_2O_4$-solid; d) $FeCo_2O_4$-solid and e) $NiCo_2O_4$-solid.

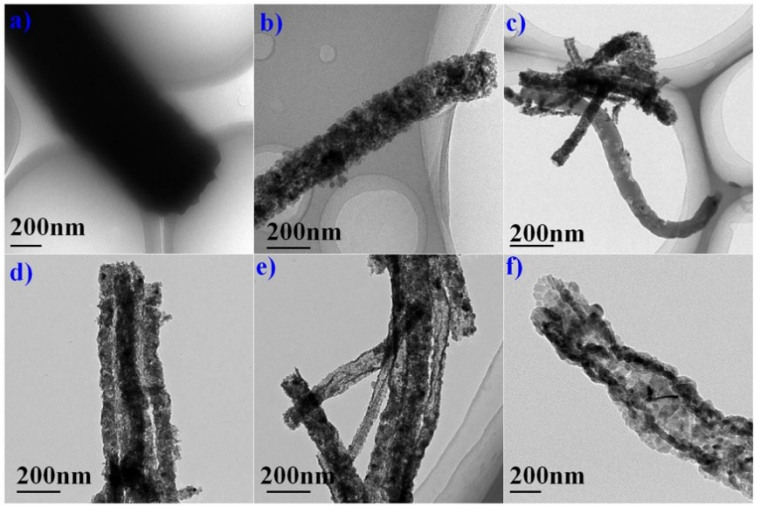

Figure S14 TEM images of prepared various mixed oxides nanostructures: (a) $NiCo_2O_4$ with 1D solid structure and hollow tubular structure of (b) $NiCo_2O_4$; (c)

$NiMn_2O_4$; (d) $FeCo_2O_4$; (e) $CuMn_2O_4$ and (f) $CoMn_2O_4$.

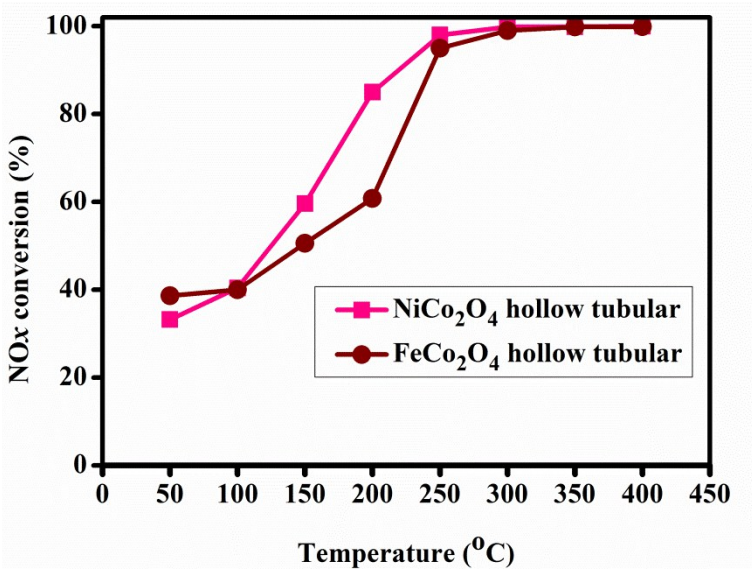

Figure S15 NO_x conversion of $FeCo_2O_4$ and $NiCo_2O_4$ with hollow tubular structures.

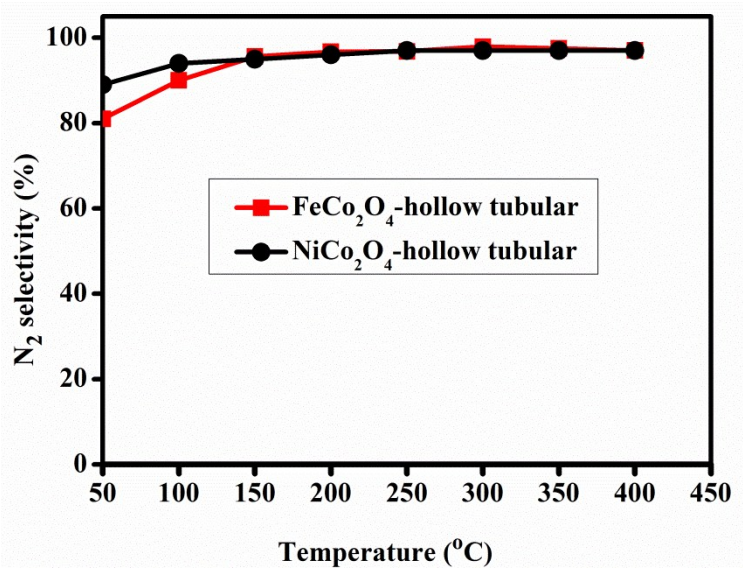

Figure S16 N_2 selectivity of $FeCo_2O_4$ and $NiCo_2O_4$ with hollow tubular structures.

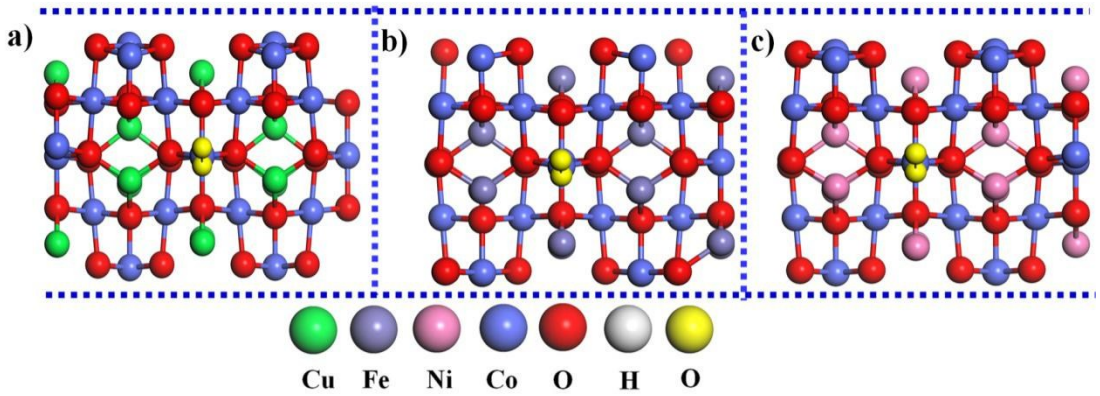

Figure S17 O_2 adsorption over the a) $CuCo_2O_4$ (220); b) $FeCo_2O_4$ (220) and c) $NiCo_2O_4$ (220) catalyst surface models.

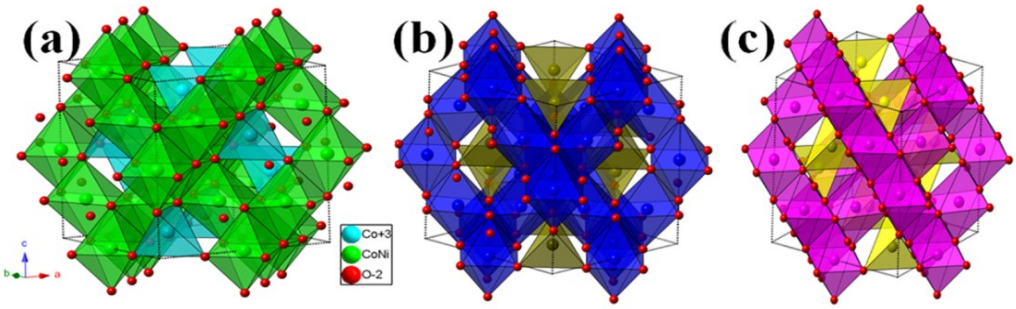

Figure S18 The simulated structures of unit cells for (a) $NiCo_2O_4$; (b) $FeCo_2O_4$ and (c) $CuCo_2O_4$.

SEM images (Figure S12) show that the precursors of $FeCo_2O_4$, $NiCo_2O_4$, $CuMn_2O_4$, $CoMn_2O_4$ and $NiMn_2O_4$ with 1D nanofibers structures can be successfully synthesized. More importantly, SEM (Figure S13) and TEM images (Figure S14) confirm that $CuMn_2O_4$, $CoMn_2O_4$, $NiMn_2O_4$, $FeCo_2O_4$ and $NiCo_2O_4$ with 1D solid and hollow tubular structures could be also tuned by controlling heating rates. These results imply that the present strategy is effective and versatile for preparing 1D solid and hollow tubular mixed transition metal oxides with different compositions. Among them, hollow tubular $NiCo_2O_4$ and $FeCo_2O_4$ were further chosen to test NH_3-SCR performance in comparison with $CuCo_2O_4$ and $CuCo_2O_4$-solid. NO_x conversion at 100-250 ^oC follows the order: $CuCo_2O_4$ > $NiCo_2O_4$ > $FeCo_2O_4$ > $CuCo_2O_4$-solid (Figure 3a and Figure S15). N_2 selectivity (Figure S16) of $NiCo_2O_4$ and $FeCo_2O_4$ is more than 95% at 100-400 ^oC. DFT calculation (Figure S17) was carried out to study the oxygen adsorption energy (E_{ads}) on (220) plane over $CuCo_2O_4$, $FeCo_2O_4$ and $NiCo_2O_4$. E_{ads} values confirm that O_2 preferentially adsorbs (Table S3) on the $CuCo_2O_4$ (220) surface rather than

$NiCo_2O_4$ (220) or $FeCo_2O_4$ (220), implying easier formation of oxygen vacancies on $CuCo_2O_4$ (220). The simulated structure of unit cell (Figure S18) in $CuCo_2O_4$ displays that Cu occupies the octahedral coordination sites. [19, 20] and the oxygen-oxygen bond length is changed when Cu is replaced by Ni or Fe. The bond length shortens in $NiCo_2O_4$ (1.290 Å) and $FeCo_2O_4$ (1.285 Å) with respect to $CuCo_2O_4$ (1.437 Å) (Table S3), which is unfavorable for the formation of oxygen vacancies. This observation agrees with the O1s XPS results.

Table S1 Textural properties and total NH_3 desorption amounts of hollow tubular $CuCo_2O_4$ and $CuCo_2O_4$-solid.

Sample	BET surface area (m^2/g)	Pore volume (cm^3/g)	The amounts of NH_3 desorption (*m*mol/g)
$CuCo_2O_4$-solid	45	0.18	1.70
$CuCo_2O_4$	72	0.23	4.34

Table S2 Surface valence state and $O_{ads}/(O_{latt}+O_{ads})$ molar ratio.

Sample	Surface valence state	$O_{ads}/(O_{latt}+O_{ads})$ (%)
$CuCo_2O_4$-solid	Cu^{2+}, Cu^{+}, Co^{2+}, Co^{3+}	54.94
$CuCo_2O_4$	Cu^{2+}, Cu^{+}, Co^{2+}, Co^{3+}	63.61
$FeCo_2O_4$	Fe^{2+}, Fe^{3+}, Co^{2+}, Co^{3+}	51.94
$NiCo_2O_4$	Ni^{2+}, Ni^{3+}, Co^{2+}, Co^{3+}	55.04

Table S3 The calculated results based on O_2 adsorption over (220) planes in $CuCo_2O_4$, $NiCo_2O_4$ and $FeCo_2O_4$.

Sample		E (eV)	$d_{metal\text{-}gas\ atom}$ (Å)	$D_{O\text{-}O}$ (Å)
$FeCo_2O_4$ (220)	E_{ads}-O_2	-1.60	1.676	1.285
$NiCo_2O_4$ (220)	E_{ads}-O_2	-1.69	1.688	1.290
$CuCo_2O_4$ (220)	E_{ads}-O_2	-2.21	2.068	1.437

References

[1] B. Thirupathi, P. G. Smirniotis, Nicked-doped Mn/TiO_2 as an Efficient Catalyst for the Low-Temperature SCR of NO with NH_3: Catalytic Evalauation and Characterizations. *J. Catal.* **2012**, *288*, 74-83.

[2] A. Grossale, I. Nova, E. Tronconi, D. Chatterjee, W. Weibel. The Chemistry of the NO/NO_2–NH_3 "fast" SCR Reaction over Fe-ZSM5 Investigated by Transient Reaction Analysis. *J. Catal.* **2008**, *256,* 312-322.